

Published in final edited form as:

*Neuron*. 2012 August 9; 75(3): 393–401. doi:10.1016/j.neuron.2012.05.026.

## Plasticity and stability of the visual system in human achiasma

M.B. Hoffmann<sup>1</sup>, F.R. Kaule<sup>1,\*</sup>, N. Levin<sup>2,\*</sup>, Y. Masuda<sup>3</sup>, A. Kumar<sup>4</sup>, I. Gottlob<sup>4</sup>, H. Horiguchi<sup>3,5</sup>, R.F. Dougherty<sup>5</sup>, J. Stadler<sup>6</sup>, B. Wolynski<sup>1</sup>, O. Speck<sup>7</sup>, M. Kanowski<sup>8</sup>, Y.J. Liao<sup>9</sup>, B.A. Wandell<sup>5</sup>, and S.O. Dumoulin<sup>10</sup>

<sup>1</sup>Ophthalmology, Otto-von-Guericke-University, Magdeburg, Germany <sup>2</sup>Neurology, Hadassah Hebrew University Medical Center, Jerusalem, Israel <sup>3</sup>Ophthalmology, Jikei University School of Medicine, Tokyo, Japan <sup>4</sup>Ophthalmology, University of Leicester, Leicester, UK <sup>5</sup>Psychology, Stanford University, Stanford, USA <sup>6</sup>Leibniz Institute for Neurobiology, Magdeburg, Germany <sup>7</sup>Biomagnetic Medical Magnetic Resonance, Physics, Otto-von-Guericke-University, Magdeburg, Germany <sup>8</sup>Neurology, Otto-von-Guericke-University, Magdeburg, Germany <sup>9</sup>Ophthalmology, Stanford University, Stanford, USA <sup>10</sup>Experimental Psychology, Helmholtz Institute, Utrecht University, Utrecht, Netherlands

### Summary

The absence of the optic chiasm is an extraordinary and extreme abnormality in the nervous system. The abnormality produces highly atypical functional responses in the cortex, including overlapping hemifield representations and bilateral population receptive fields in both striate and extrastriate visual cortex. Even in the presence of these large functional abnormalities, the effect on visual perception and daily life is not easily detected. Here we demonstrate that in two achiasmic humans the gross topography of the geniculo-striate and occipital callosal connections remains largely unaltered. We conclude that visual function is preserved by reorganization of intra-cortical connections instead of large-scale reorganizations of the visual cortex. Thus developmental mechanisms of local wiring within cortical maps compensate for the improper gross wiring to preserve function in human achiasma.

### Keywords

Retinotopy; population receptive fields; DTI; tractography; V1; modelling; plasticity; stability; achiasmia

---

Ordered maps of the contralateral visual field are presumed imperative for proper visual system function, and are a core principle of the notion of hemispheric specialization (Huberman et al., 2008; Wandell et al., 2007). A prerequisite for this map formation in animals with binocular vision is a partially crossed projection of the optic nerves at the optic chiasm. Here axons from the nasal and temporal retinae are guided by molecular markers to the contralateral and ipsilateral hemisphere, respectively (Petros et al., 2008). There they form a retinotopic map of the visual hemifield contralateral to the respective hemisphere

---

© 2012 Elsevier Inc. All rights reserved.

Correspondence to: S.O. Dumoulin.

\*These authors contributed equally

**Publisher's Disclaimer:** This is a PDF file of an unedited manuscript that has been accepted for publication. As a service to our customers we are providing this early version of the manuscript. The manuscript will undergo copyediting, typesetting, and review of the resulting proof before it is published in its final citable form. Please note that during the production process errors may be discovered which could affect the content, and all legal disclaimers that apply to the journal pertain.

(Figure 1A and supplementary Figure 1). In congenital achiasma, this crossing is absent providing large-scale erroneous input to the visual system (Apkarian et al., 1994; Apkarian et al., 1995; Victor et al., 2000; Williams et al., 1994). Both hemiretinae project to the ipsilateral hemisphere, which as a consequence receives input not only from the contralateral, but also from the ipsilateral visual hemifield. This poses a substantial challenge to the organization of visual field maps and prompts potential sensory conflicts. Despite these sizable aberrant projections, achiasmic humans have relatively normal visual function (Apkarian et al., 1994; Apkarian et al., 1995; Prakash et al., 2010; Victor et al., 2000). Therefore achiasma offers a unique opportunity to study the principles governing cortical map development in humans. The knowledge of cortical mapping in this condition would provide insights into scope and mechanisms of developmental plasticity in the human visual system.

The organization of the visual cortex and of the visual pathways beyond the lateral geniculate nucleus (LGN) in achiasma is unknown as only very few studies addressed related issues (Victor et al., 2000; Williams et al., 1994). A study in a canine model of achiasma investigated the precise mapping of information in the visual system, but it was confined to the level of the LGN. Here retinotopic maps of opposing hemifields in adjacent LGN layers were revealed (Williams et al., 1994). Another pioneering study addressed the cortical organization in human achiasma using functional magnetic resonance (fMRI) (Victor et al., 2000). This case study suggested that stimuli in opposing visual hemifields are represented in close cortical vicinity, but visual field map representations could not be reconstructed. To date the geniculo-striate projections (LGN-striate or optic radiations), cortico-cortical projections and the corresponding cortical organization pattern are still obscure in achiasma, such that the developmental mechanisms that make the abnormal visual input available for visual perception remain unknown. An idea of the cortical organization patterns to be expected, however, can be inferred from visual field representations in albinism, where part of the temporal retina projects abnormally to the contralateral hemisphere (Guillery, 1986). Thus input from both hemifields reaches each hemisphere. In fact, in albinism three different resulting cortical organization patterns have been reported. The geniculo-striate projection can be reordered resulting in a contiguous retinotopic map of both visual hemifields (“Boston” pattern); alternatively reordering can be absent with intra-cortical suppression inducing a lack of behavioural sensitivity of the temporal retina (“Midwestern” pattern), or without suppression retaining sensitivity (“True Albino” pattern). While the former organization patterns of the visual cortex appear to be reserved to non-primate models of albinism, the latter is found in both non-primates and primates (Guillery et al., 1984; Hoffmann et al., 2003). Our aim was to resolve the organization pattern in human achiasma.

We investigated two of these extremely rare achiasmic subjects. Three types of investigations were performed using 1.5, 3 and 7 Tesla MRI, (1) optimized retinotopic mapping (DeYoe et al., 1996; Engel et al., 1997; Engel et al., 1994; Hoffmann et al., 2009; Sereno et al., 1995; Wandell et al., 2007), (2) characterization of the population receptive field (pRF) properties (Dumoulin and Wandell, 2008), and (3) diffusion-tensor imaging (DTI) and tractography to investigate white matter integrity (Sherbondy et al., 2008a; Sherbondy et al., 2008b). Our results indicate that the abnormal visual input in human achiasma does not induce a sizable topographic reorganization in the geniculo-striate projection or of the occipital callosal connections. We propose that reorganization of intra-cortical architecture in the visual system underlies the ability to cope with these abnormal inputs.

## Results

### Hemifield mapping reveal overlapping visual field maps

In subject AC1, visual hemifield representations on the cortical surface were obtained separately for each visual hemifield and eye using fMRI-based retinotopic mapping (DeYoe et al., 1996; Engel et al., 1997; Engel et al., 1994; Hoffmann et al., 2009; Sereno et al., 1995; Wandell et al., 2007). Mapping of either visual hemifield yielded dominant responses on the occipital lobe ipsilateral to the stimulated eye (Figure 1 and supplementary Figure S1). Figure 1 illustrates that stimulation of the right eye revealed orderly eccentricity maps of both hemifields on the right hemisphere only (Figure 1B). Moreover, opposite visual hemifields were represented as a cortical superposition of mirror-symmetrical visual field positions. Accordingly, the phase-maps obtained for stimulation in opposite hemifields were highly correlated (Figure 1C) and the borders of the early visual areas were identical for the representation of the contralateral and the ipsilateral visual hemifield as derived from polar angle maps (supplementary Figure S1). Similar results were obtained on the left hemisphere for stimulation of the left eye (supplementary Figure S1).

### PRF mapping reveals bilateral population receptive fields

The above results predicted that in the visual cortex of achiasmatic humans, neural populations within an fMRI recording site have bilateral receptive fields (population receptive fields, pRFs), receiving distinct inputs from the contra- and the ipsilateral visual hemifield. To test this directly, we extended a novel model-based data-analysis technique to estimate the properties of the pRF (Dumoulin and Wandell, 2008). The stimuli consisted of moving bar apertures covering both visual hemifields. The conventional pRF model consists of a circularly symmetric 2D Gaussian, whose resulting parameter estimates vary systematically across visual cortex and match closely to non-human primate electrophysiology (Amano et al., 2009; Dumoulin and Wandell, 2008; Harvey and Dumoulin, 2011; Winawer et al., 2010). We compared four models of the pRF: the conventional 2D Gaussian pRF model and three additional models that consisted of two 2D Gaussians. The two 2D Gaussians were identical, except that their positions were either mirrored around the vertical meridian, fixation or horizontal meridian. Because all parameters of the two Gaussians were linked, these new models have the same degrees of freedom as the conventional one Gaussian pRF model, i.e. the model performance can be compared directly. But unlike the conventional model, the three alternate models predict that each cortical location responds to stimuli from two distinct regions of visual space. We compared the four models by computing the average goodness-of-fit, i.e. variance explained, within the right Calcarine sulcus. Both achiasmatic subjects were included in this analysis.

For both achiasmatic subjects in the right Calcarine sulcus, the pRF model consisting of two Gaussians mirrored across the vertical-meridian explained most of the variance, whereas for control subjects the conventional pRF model explained most of the variance in the data (Figure 2A). Inspection of individual fMRI time-series of the achiasmatic subject (AC2), indicate that the pRF model consisting of two Gaussians captures systematic signal modulations that the conventional model cannot explain (Figure 2B,C). These improvements are evident for most individual recording sites across the cortical surface extending beyond V1, again in contrast with control subjects (Figure 2D,E). Another line of evidence supporting the notion that achiasmatic subjects have symmetric pRFs both in contra and ipsilateral visual hemifield comes from pRF sizes. The pRF size properties are comparable to controls, only when considering the atypical pRF model consisting of two Gaussians mirrored across the vertical meridian (Figure 2F and supplementary Figure S2). The pRF sizes across early visual cortex in conjunction with the persistence of dual receptive fields

into extra-striate cortex, also implies relatively unaltered cortico-cortical connections (Harvey and Dumoulin, 2011).

### DTI and tractography reveal relatively normal white matter tracts

Since each hemisphere contains information of the whole visual field in achiasma, we questioned whether the two hemispheres needed to communicate to the same degree. Therefore we investigated the visual pathway connectivity including the occipital callosal connections. A previous study demonstrated the sensitivity of these connections to alterations of the visual input (Levin et al., 2010). Visual pathways white matter analysis was performed in two steps: identifying the fiber bundles and evaluating their properties. Using a new probabilistic algorithm (Sherbondy et al., 2008a; Sherbondy et al., 2008b), we could clearly identify the *optic tract* and the *optic radiation* composing the input fibers to the visual cortex as well as the output fibers from each hemisphere, which cross at the corpus callosum (Figure 3A). Following fiber identification, we studied white matter integrity using directional diffusivity measures. By measuring diffusivity in multiple directions we obtained estimates of the principal diffusion direction (longitudinal) as well as the perpendicular direction (radial). The ratio of these two values is similar to the fractional anisotropy (FA). We found that the properties of the achiasmic subject's (AC2) visual pathways were within the range of 30 normally sighted control subjects (Figure 3B). Finally, the cross-sectional area of the occipital fibers that connect right and left visual cortex was assessed (Figure 3C). In normal sighted controls there is a correlation between the cross-sectional area of this tract and the cross-sectional area of the entire callosum. The cross-sectional area of the achiasmic subject's occipital callosal fiber group was smaller than that of controls, yet the overall size of his corpus callosum was small too (Figure 3D). These results highlight that the white matter integrity at the resolution of our neuroimaging measurements is comparable to control subjects.

### Discussion

Our results highlight both differences and similarities of the achiasmic compared to the typical human visual system. In achiasma, we found a highly atypical organization of the visual cortex consisting of overlapping visual hemifield maps with bilateral pRFs. In contrast, pRF sizes were in the normal range as were the properties of all major visual pathways, in particular the geniculate-cortical and occipital-callosal fibers. Moreover, normal pRF sizes across early visual cortex in conjunction with the persistence of bilateral pRFs imply relatively unaltered cortico-cortical connections (Harvey and Dumoulin, 2011).

### Conservative geniculo-striate projections in human achiasma

Our results can be explained by conservative developmental mechanisms in human achiasma that largely preserve the normal visual pathways beyond the LGN. Both retinotopic and pRF mapping demonstrated an overlay of orderly retinotopic maps from opposing hemifields in the visual cortex, such that each cortical location represents two separate visual field locations, namely one in each hemifield. This intermixed representation could result from individual neurons with bilateral receptive fields, but also from the interdigitation of two different neural populations representing the contra- and ipsilateral visual field at the current fMRI resolution. These two neural representations are not mutually exclusive. In support of the latter, behaviourally achiasmic subjects do not make any obvious confusion between visual hemifields in line with previous reports (Victor et al., 2000). Furthermore, Williams et al. (Williams et al., 1994) demonstrated that in the only animal model of achiasma, the Belgian sheepdog, the different layers of the LGN receive input from the ipsilateral eye of either the contra- or the ipsilateral visual hemifield. As a consequence, a conservative geniculo-striate projection would yield interdigitated

representations of the contra- and ipsilateral fields in V1, as those would occupy the former ocular dominance columns (Guillery, 1986; Huberman et al., 2008). This corresponds to the intermixed cortical visual field representations we observed. Thus the data are in support of largely conservative geniculo-striate pathways in achiasma preserving the normal gross topography of the projections. This is further corroborated by the normal gross anatomy of the optic radiations as determined using DTI and tractography. It should be noted, however, that the data do not speak to the fine-grained organization in V1 in achiasma. Thus it is not clear whether the afferents from the different LGN layers organize themselves into structures reminiscent of ocular-dominance columns, namely into hemifield columns. In conclusion, the highly atypical functional responses in V1 appear to be a consequence of the gross miss-wiring at the chiasm without corresponding changes in the gross wiring of the geniculo-striate projection.

### **Conservative cortico-cortical projections in human achiasma**

Beyond V1, cortico-cortical connections remain stable as indicated by normal pRF sizes in both striate and extra-striate cortex (Harvey and Dumoulin, 2011) and the persistence of bilateral pRFs in extra-striate cortex. Even interhemispherical connections appear little affected, as stable normal occipital callosal connections were observed. The finding that the representation error in the LGN is propagated in an unaltered manner to the primary visual cortex and beyond, highlights the dominance of conservative developmental mechanisms in human achiasma.

### **Developmental mechanisms associated with visual pathway abnormalities**

The mapping of the abnormal input observed in achiasma resembles that of human and non-human primates with completely different types of misrouting, namely abnormal crossing from the temporal retina in albinotic subjects (Guillery, 1986; Hoffmann et al., 2003) or an absence of crossing due to a prenatal hemispheric lesion (Muckli et al., 2009). In contrast, a variety of organization patterns in V1 have been reported for non-primate albinotic animal models of misrouted optic nerves, part of which involves sizable remapping (Guillery, 1986). In the human visual cortex such large scale remapping does not appear to be a prevalent strategy to avoid sensory conflicts (Hoffmann et al., 2007; Wolynski et al., 2010).

### **Visual perception**

Our results demonstrate a remarkable degree of both stability and plasticity in human achiasma. The observed cortical organization with overlapping visual hemifield maps with bilateral pRFs is highly atypical and the consequence of a large degree of stability in the geniculo-striate and cortico-cortical projections. Still visual function is relatively unaffected, with the exception of nystagmus and the absence of stereopsis. In line with previously reported achiasmatic subjects (Apkarian et al., 1994; Apkarian et al., 1995; Prakash et al., 2010; Victor et al., 2000), the subjects made effective use of their vision in daily life, including sport activities and reading. They performed normal on various clinical tasks, including largely normal visual field sensitivities and no visual field defects associated with the abnormal representation of the nasal retina. Further, there was no apparent confusion between left and right visual fields in line with previous reports that have found no evidence for perceptual crosstalk across the opposing hemifields, neither in achiasma (Victor et al., 2000) nor albinism (Klemen et al., 2012).

In order to make the abnormally represented visual information available for perception neural plasticity is required. We propose that instead of large-scale reorganizations, comparatively subtle intra-cortical mechanisms mediate the achiasmatic subjects' ability to cope with the abnormal visual input. For example, normally binocular information is integrated to yield stereo-vision. In achiasma, however, these integrative mechanisms would



result in major sensory conflicts such as confusions between the two hemifields. Plasticity of intra-cortical mechanisms is therefore required to selectively block such integrative processes while supporting others, e.g. those required to shape monocular spatial receptive field properties. Remarkably, conservative geniculostriate and cortico-cortical mapping of abnormal retino-geniculate input provides a sufficient scope of developmental plasticity in humans to make substantially abnormal representations available for relatively normal visual perception.

## Experimental Procedures

### Subjects

Data of two male achiasmic patients and their respective controls were acquired at two sites, at Magdeburg University, Germany (AC1 and four controls) and Stanford University, USA (AC2 and 34 controls). The control subjects were visually and neurologically normal. The procedures followed the tenets of the declaration of Helsinki and the participants gave their written consent. The ethical committees of University of Magdeburg, Germany and Stanford Institutional Review Board, USA approved the respective protocols.

AC1 (aged 22) was referred with the clinical diagnosis of severe hypoplasia of the optic chiasm based on a T1 weighted MRI and functional achiasma was confirmed with VEPs (Apkarian et al., 1995; Apkarian et al., 1983). He made effective use of his vision including reading and the diagnosis of the chiasmic malformation was incidental (age 20). His best-corrected decimal visual acuity was 0.5 for the dominant right and 0.17 for the left eye, and there was no foveal hypoplasia. He had alternating exotropia (2 deg), dissociated vertical deviation (5 deg) and was stereoblind. Automated perimetry (Octopus 101 Perimeter; Haag-Streit, Koeniz, Switzerland) with optimized protocols (Hoffmann et al., 2007) revealed normal visual fields. Specifically no visual field defects were associated with the nasal retina, and visual field sensitivities did not differ between nasal and temporal hemiretinae of the dominant right eye (mean sensitivities  $\pm$  SEM [dB] for nasal and temporal hemiretina (n=47 test locations each)  $25.9\pm 0.37$  and  $25.5\pm 0.46$ , respectively;  $p=0.48$ , paired t-Test). The subject exhibited normal visual and visuo-motor behavior throughout testing. There was no left-right confusion as tested for saccadic eye movements (100% correct saccades to 12 targets in the right and 12 in the left visual hemifield, displaced laterally 5.8 deg from a central fixation target). Moderate see-saw nystagmus (around 3 deg horizontal and vertical amplitude for the right eye) was evident. It has been shown previously that fixation instabilities of such moderate extent have only little effect on the visual field map reconstruction (Baseler et al., 2002; Levin et al., 2010). The left eyes of the four male control subjects and both eyes of AC1 were stimulated monocularly during the retinotopic hemifield mapping experiments. A control's and AC1's right eye were also measured for pRF mapping.

AC2 (aged 30) has been described in detail in a previous publication (Prakash et al., 2010). In summary, the subject was born with a non-random association of birth defects known as VACTERL (Vertebral anomalies, Anal atresia, Cardiovascular anomalies, Tracheoesophageal fistula, Esophageal atresia, Renal and/or radial anomalies and Limb anomalies). Appendicular abnormalities were surgically repaired. As a child, he had mild infantile nystagmus with relatively normal visual function. He had been diagnosed with attention deficit disorder as a child and bipolar affective disorder as an adult. Even so, he completed high school and worked full-time. He also made effective use of his vision including during sport activities and reading. At 29 he was evaluated for a two-year history of gradually worsening headache, blurred vision and increased nystagmus amplitude and the diagnosis of achiasma was made at this time by brain MRI and fMRI showing functional non-crossing of the visual pathway. On examination, his visual acuities were 1.0 and 0.8 in

the right and left eye, respectively, with a small left relative afferent pupillary defect. Anterior and posterior segments were normal. The subject's eye movements had full duction, normal saccade latencies, amplitudes, and peak velocities. He exhibited pendular nystagmus and episodic seesaw nystagmus, which were relatively minimal during the current fMRI studies (age 30). Stereopsis was absent. Color perception was within normal limits per Hardy-Rand-Rittler pseudoisochromatic plates. There was no left-right confusion or neglect per clinical testing using visual stimuli in nasal or temporal fields or simultaneously to one or both eye. Goldmann perimetry revealed slightly constricted visual fields bilaterally with no evidence of temporal or other visual field defect.

### Hemifield mapping

**Visual stimuli**—For retinotopic hemifield mapping (DeYoe et al., 1996; Engel et al., 1997; Engel et al., 1994; Sereno et al., 1995) a section of a contrast reversing circular checkerboard stimulus (6 reversals/s, 90 cd/m<sup>2</sup> mean luminance) presented in a rectangular mask (30 deg wide and 15 deg high, Figure 1A) was used to stimulate monocularly either the nasal or the temporal retina in separate experiments. The stimulus contrast was set to 98% in the hemifield to be mapped, and to 0% in the opposing hemifield. Seven 36 s cycles of the stimulus stepping either through the polar angles (clock- and counterclockwise for the left and right hemifield, respectively) as a rotating wedge (90 deg) for polar angle mapping or through the eccentricities as a contracting ring for eccentricity mapping (ring width: 0.82 deg; ring was off-screen entirely for 7 s of the 36 s stimulus cycle before reappearing in the periphery) were projected (DLA-G150CL, JVC Ltd.) on a screen using Presentation (NeuroBehavioral Systems). For eccentricity and polar angle mapping we collected for each subject and each hemifield two datasets, which were averaged for subsequent analyses. During stimulation subjects were instructed to maintain fixation and to report color changes of the central target (diameter: 0.25 deg) via button press. Fixation was monitored during the scans with an MR-compatible eye tracker (Kanowski et al., 2007).

**Data acquisition**—To enhance the signal-to-noise-ratio as well as the Blood Oxygenation Level Dependent (BOLD) response, T2\*-weighted MR-images were acquired during visual stimulation using a Siemens Magnetom 7T MRI system with a 24-channel-coil (Hoffmann et al., 2009). Foam padding minimized head motion. A multi-slice 2D gradient echo EPI sequence (TR 2.4 s; TE 22 ms) was used to measure the BOLD signal as a function of time. Every 2.4 s 42 approximately axial slices (thickness: 2.5 mm; interleaved slice order without gap) were acquired in an 80 × 80 grid covering a field of view (FOV) of 200 × 200 mm (voxel size: 2.5 × 2.5 × 2.5 mm<sup>3</sup>). Functional scans measured at 110 time frames (4.4 min, i.e., 7 1/3 stimulus cycles of 36 s each). The acquired images were motion and distortion corrected online (Zaitsev et al., 2004). Additionally, T1 weighted MPRAGE MR images (Van de Moortele et al., 2009) were acquired (TR 2.0 s; TE 5.24 s, 176 × 256 × 256 matrix, voxel size: 1 × 1 × 1 mm<sup>3</sup>) to create a flattened representation of the cortical grey matter (Teo et al., 1997; Wandell et al., 2000).

**Data analysis**—After registration of the T1 weighted images to the T2\* weighted images' co-ordinate frame the fMRI time series were projected onto the flattened representation (Engel et al., 1997). Each voxel's time-series (TS) underwent the following analysis: (1) Five temporal samples were discarded from the TS to avoid transient onset artifacts, (2) the TS were divided by the voxel's mean intensity, (3) the TS were filtered with a high-pass cut-off of 4 cycles/scan, (4) the TS of repeated experiments were averaged, (5) Fourier analysis was applied to the TS to obtain the amplitude and phase for each frequency, and (6) the coherence with a sinusoid with a frequency equal to that of the visual stimulation (1/36 Hz), was calculated (Engel et al., 1997). The coherence and phase values in the flattened representation were blurred by convolving a Gaussian kernel (1.7 mm full width at half

height) with the complex vector representation of the BOLD response. The blurred phase values that exceeded a coherence threshold that corresponded to  $p < 0.001$  (Silver et al., 2005) were then plotted on the flattened representation of the occipital lobe in false color.

**Statistics**—To assess the correlation of the hemifield maps, the significance of the differences of the z-transformed correlation coefficients (Berens, 2009) from 0 were determined with Student's t-test.

### PRF model-based analysis

**Visual stimuli**—We measured responses to drifting bar apertures at various orientations (Dumoulin and Wandell, 2008); these bar apertures exposed a checkerboard pattern (100% contrast). The bar width subtended  $1/4^{\text{th}}$  of the stimulus radius. Four bar orientations and two different motion directions for each bar were used, giving a total of 8 different bar configurations within a given scan. Note that the bars were not “phase-encoded” stimuli; there was no repetition of the stimulus because the bars change orientation and motion direction within a scan. The visual stimuli were generated in the Matlab programming environment using the PsychToolbox (Brainard, 1997; Pelli, 1997) on a Macintosh G4 Powerbook. Stimuli were displayed with an LCD projector (Stanford: NEC LT158, Magdeburg: DLA-G150CL, JVC Ltd.) with optics that imaged the stimuli onto a projection screen in the bore of the magnet. The stimulus radius was 7.5 deg (Magdeburg setup for AC1) and 14 deg (Stanford setup for AC2) of visual angle. The subjects viewed the display through an angled mirror. Fixation was monitored during the scans with an MR-compatible eye tracker (Magdeburg: Kanowski et al., 2007; Stanford: MagConcept, Redwood City, USA).

**Data acquisition**—At Stanford University, magnetic resonance images were acquired with a 3T General Electric Signa scanner and a custom-designed surface coil (Nova Medical, Wilmington, MA) centered over the subject's occipital pole. Foam padding and tape minimized head motion. Functional MR images (TR 1.5 s; TE 30 ms, flip angle 55 deg) were acquired using a self-navigated spiral-trajectory pulse sequence (Glover, 1999; Glover and Lai, 1998) with 20 slices oriented orthogonal to the Calcarine sulcus with no slice gap. The effective voxel size was  $2.5 \times 2.5 \times 3 \text{ mm}^3$  (FOV =  $240 \times 240 \text{ mm}$ ). Functional scans measured at 138 time frames (3.5 min). Eight functional scans were performed in each session. T1-weighted anatomical MR images were acquired using a fast spoiled gradient echo (SPGR) sequence prior to the functional scans and using the same slice prescription as the functional scans. In a separate session high-resolution T1-weighted MRI images were acquired on a 1.5T Signa LX scanner with a vendor-supplied head-coil using a 3D-SPGR pulse sequence (1 echo, minimum TE, flip angle 15 deg, effective voxel size of  $0.94 \times 0.94 \times 1.2 \text{ mm}^3$ ). At the Magdeburg site, images for fMRI-based pRF-mapping were acquired using a Siemens Magnetom 7T MRI system with the hemifield mapping parameters detailed above, except for the following deviations for similarity to the Stanford parameters: 26 slices, 138 time frames, TR 1.5 s.

**Data analysis**—For the data acquired at Stanford University the T1-weighted anatomical MRI data sets were averaged and re-sampled to a  $1 \text{ mm}^3$  isotropic resolution. The surface-coil anatomical MRI, taken at the same time as the functional images, was aligned with the head-coil anatomical MRI using a mutual information method (Ashburner and Friston, 2003; Maes et al., 1997). The functional images and surface-coil anatomical data acquired in the same session and thus were co-registered. Using the spiral acquisition and small field of view surface-coil limits the size of the distortions between the functional and surface-coil anatomical images. Hence, we used the transformation derived from the surface-coil anatomical to align the functional data to the head-coil anatomical. The preprocessing for



the data acquired at Magdeburg University followed that applied to the hemifield mapping data described above. For both data sets gray and white matter was segmented from the anatomical MRI using custom software and hand-edited to minimize segmentation errors (Teo et al., 1997). The cortical surface was reconstructed at the white/gray matter border and rendered as a smoothed 3D surface (Wandell et al., 2000). The first 8 time-frames of each functional run were discarded due to start-up magnetization transients. Head movement and motion artifacts within and between scans were measured (Nestares and Heeger, 2000). With all subjects, the scans contained minimal head motion (less than one voxel), so no motion correction algorithm was applied. The population receptive field (pRF) is defined as the region of visual space that stimulates the recording site (Dumoulin and Wandell, 2008; Jancke et al., 2004; Victor et al., 1994). We used a model-based method to estimate the properties of the pRF. Details of the pRF analysis and rationale are provided in our previous study (Dumoulin and Wandell, 2008). Briefly, for each cortical location we predicted the fMRI response using a model of the pRF. The conventional model consists of a 2D Gaussian. The predicted fMRI time-series is calculated by a convolution of the model pRF with the stimulus sequence and the BOLD hemodynamic response function (HRF); the pRF parameters for each cortical location minimize the sum of squared errors between the predicted and observed fMRI time-series for all stimuli. Here we tested several other models of the pRF in addition to the conventional 2D Gaussian. These models consisted of two 2D Gaussians mirrored around the x-axis, y-axis or fixation. Because the two Gaussians are linked to each other, these models have the same degrees of freedom as the conventional one Gaussian pRF model. But unlike the conventional model, these alternate models represent two distinct regions of visual space within each cortical location.

### DTI and tractography

**Data acquisition**—DTI data were acquired on a 1.5T Signa LX (Signa CVi; GE Medical Systems, Milwaukee, WI) with a self-shielded, high-performance gradient system capable of providing a maximum gradient strength of 50 mT/m at a gradient rise time of 268  $\mu$ s for each of the gradient axes. A standard quadrature head coil was used for excitation and signal reception. The DTI protocol used eight 90-sec whole-brain scans. The pulse sequence was a diffusion-weighted, single-shot, spin-echo, echo-planar imaging sequence (echo time, 63 msec; repetition time, 6 sec; field of view, 260 mm; matrix size, 128  $\times$  128; bandwidth,  $\pm$ 110 kHz; partial k-space acquisition). We acquired 48–54 axial, 2-mm-thick slices (no skip) for two  $b$ -values,  $b = 0$  and  $b = 800$  sec/mm<sup>2</sup>. The high  $b$ -value was obtained by applying gradients along 12 different diffusion directions (six noncollinear directions). Two gradient axes were energized simultaneously to minimize echo time. The polarity of the effective diffusion-weighting gradients was reversed for odd repetitions to reduce cross-terms between diffusion gradients and imaging and background gradients.

**Data analysis**—Eddy current distortions and subject motion were removed by a 14-parameter constrained non-linear co-registration based on the expected pattern of eddy-current distortions given the phase-encode direction of the acquired data (Rohde et al., 2004). Each diffusion-weighted image was then registered to the mean of the (motion-corrected) non diffusion-weighted images using a two-stage coarse-to-fine approach that maximized the normalized mutual information. The mean of the non-diffusion weighted images was also automatically aligned to the T1 image using a rigid body mutual information algorithm. All raw images from the diffusion sequence were then re-sampled to 2 mm isotropic voxels by combining the motion correction, eddy-current correction, and anatomical alignment transforms into one omnibus transform. and re-sampling the data using a 7th-order b-spline algorithm based on code from SPM5 (Friston and Ashburner, 2004) was done. An eddy-current intensity correction (Rohde et al., 2004; Rohde et al., 2005) was also applied to the diffusion weighted images at this re-sampling stage. The

rotation component of the omnibus coordinate transform was applied to the diffusion-weighting gradient directions to preserve their orientation with respect to the re-sampled diffusion images. The tensors were fit using a least-squares algorithm. The eigenvalue decomposition of the diffusion tensor was computed, and the fractional anisotropy was calculated from the eigenvalues (Basser, 1995; Basser and Pierpaoli, 1996). The FA is the normalized standard deviation of the three eigenvalues and indicates the degree to which the isodiffusion ellipsoid is anisotropic. The mean diffusivity (MD) is the mean of the three eigenvalues, which is equivalent to one-third of the trace of the diffusion tensor.

**Tractography**—We identified the fibers using the probabilistic ConTrack algorithm (Sherbondy et al., 2008a). This method is designed to find the most likely pathway between two regions of interest and has been validated against gold-standard post-mortem tract-tracing methods (Sherbondy et al., 2008b). *Optic tract*: Large ROIs that contain the optic chiasm, including both optic tract origins, were positioned on T1 maps of each subject, centered at the infundibular stem of the hypothalamus. This way we were able to compare the optic tracts of the subject who lack an optic chiasm and the controls. Both LGNs were also defined anatomically on the T1 maps, and their volumes were standardized to 485 mm<sup>3</sup>. ConTrack calculated the most likely pathway between the ROIs of the optic chiasm and the LGN. A set of 5000 potential pathways were generated and the top 10% (500) highest scores fibers were chosen as the most likely pathways connecting these two regions. *Optic radiation*: In this case we estimated the optic radiation as the most likely pathway between the LGN ROI and each hemisphere Calcarine. The Calcarine ROIs were delineated for each subject on their T1 maps. We sampled 100,000 possible pathways and estimated the optic radiation as the top 1% (1000) of these pathways. A few clearly misidentified fibers were eliminated (Sherbondy et al., 2008b). *Occipital callosal fibers*: To analyze diffusion properties in the corpus callosum, we adopted parts of the corpus callosum segmentation procedure described by Dougherty et al. (Dougherty et al., 2007) and Huang et al. (Huang et al., 2005). We manually defined an occipital ROI within the white matter and a corpus callosum ROI for each subject. We sampled 100,000 fibers that pass through both ROIs and estimated the 1% (1000) of these generated pathways. We then measured the cross-sectional area of these callosal-occipital fibers in the plane of the corpus callosum. The process was performed on each hemisphere separately; we also estimated the cross-sectional area of the whole corpus callosum.

## Supplementary Material

Refer to Web version on PubMed Central for supplementary material.

## Acknowledgments

We thank the subjects for their patience and cooperation. We would also like to express our appreciation to Greg Corrado and Julian Brown for the use of their eye-tracker and their help. This work was supported by German Research Foundation (DFG) HO 2002/10-1 (M.B.H.), NIH EY 03164 (B.A.W.) and Marie Curie Reintegration Grant #231027 (S.O.D.).

## Abbreviations

<b>V</b>	visual area
<b>LO</b>	lateral occipital area
<b>d</b>	dorsal
<b>v</b>	ventral

<b>m</b>	medial
<b>l</b>	lateral
<b>R</b>	right hemisphere
<b>L</b>	left hemisphere
<b>c</b>	visual hemifield contralateral to right V1
<b>i</b>	visual hemifield ipsilateral to right V1

## References

- Amano K, Wandell BA, Dumoulin SO. Visual field maps, population receptive field sizes, and visual field coverage in the human MT+ complex. *Journal of neurophysiology*. 2009; 102:2704–2718. [PubMed: 19587323]
- Apkarian P, Bour L, Barth PG. A unique achiasmatic anomaly detected in non-albinos with misrouted retinal-fugal projections. *The European journal of neuroscience*. 1994; 6:501–507. [PubMed: 8019686]
- Apkarian P, Bour LJ, Barth PG, Wenniger-Prick L, Verbeeten B Jr. Non-decussating retinal-fugal fibre syndrome. An inborn achiasmatic malformation associated with visuotopic misrouting, visual evoked potential ipsilateral asymmetry and nystagmus. *Brain*. 1995; 118(Pt 5):1195–1216. [PubMed: 7496780]
- Apkarian P, Reits D, Spekreijse H, Van Dorp D. A decisive electrophysiological test for human albinism. *Electroencephalogr Clin Neurophysiol*. 1983; 55:513–531. [PubMed: 6187545]
- Ashburner, J.; Friston, KJ. Rigid body registration. In: Penny, WD., editor. *Human Brain Function*. Academic Press; 2003.
- Baseler HA, Brewer AA, Sharpe LT, Morland AB, Jagle H, Wandell BA. Reorganization of human cortical maps caused by inherited photoreceptor abnormalities. *Nature neuroscience*. 2002; 5:364–370.
- Basser PJ. Inferring microstructural features and the physiological state of tissues from diffusion-weighted images. *NMR in biomedicine*. 1995; 8:333–344. [PubMed: 8739270]
- Basser PJ, Pierpaoli C. Microstructural and physiological features of tissues elucidated by quantitative-diffusion-tensor MRI. *Journal of magnetic resonance*. 1996; 111:209–219. [PubMed: 8661285]
- Berens B. CircStat: A MATLAB Toolbox for Circular Statistics. *Journal of Statistical Software*. 2009; 31:1–21.
- Brainard DH. The Psychophysics Toolbox. *Spatial vision*. 1997; 10:433–436. [PubMed: 9176952]
- DeYoe EA, Carman GJ, Bandettini P, Glickman S, Wieser J, Cox R, Miller D, Neitz J. Mapping striate and extrastriate visual areas in human cerebral cortex. *Proceedings of the National Academy of Sciences of the United States of America*. 1996; 93:2382–2386. [PubMed: 8637882]
- Dougherty RF, Ben-Shachar M, Deutsch GK, Hernandez A, Fox GR, Wandell BA. Temporal-callosal pathway diffusivity predicts phonological skills in children. *Proceedings of the National Academy of Sciences of the United States of America*. 2007; 104:8556–8561. [PubMed: 17483487]
- Dumoulin SO, Wandell BA. Population receptive field estimates in human visual cortex. *NeuroImage*. 2008; 39:647–660. [PubMed: 17977024]
- Engel SA, Glover GH, Wandell BA. Retinotopic organization in human visual cortex and the spatial precision of functional MRI. *Cereb Cortex*. 1997; 7:181–192. [PubMed: 9087826]
- Engel SA, Rumelhart DE, Wandell BA, Lee AT, Glover GH, Chichilnisky EJ, Shadlen MN. fMRI of human visual cortex. *Nature*. 1994; 369:525. [PubMed: 8031403]
- Friston KJ, Ashburner J. Generative and recognition models for neuroanatomy. *NeuroImage*. 2004; 23:21–24. [PubMed: 15325348]
- Glover GH. Simple analytic spiral K-space algorithm. *Magn Reson Med*. 1999; 42:412–415. [PubMed: 10440968]

- Glover GH, Lai S. Self-navigated spiral fMRI: interleaved versus singleshot. *Magn Reson Med*. 1998; 39:361–368. [PubMed: 9498591]
- Guillery RW. Neural abnormalities of albinos. *Trends in neurosciences*. 1986; 9:364–367.
- Guillery RW, Hickey TL, Kaas JH, Felleman DJ, Debruyn EJ, Sparks DL. Abnormal central visual pathways in the brain of an albino green monkey (*Cercopithecus aethiops*). *The Journal of comparative neurology*. 1984; 226:165–183. [PubMed: 6330179]
- Harvey BM, Dumoulin SO. The Relationship between Cortical Magnification Factor and Population Receptive Field Size in Human Visual Cortex: Constancies in Cortical Architecture. *J Neurosci*. 2011; 31:13604–13612. [PubMed: 21940451]
- Hoffmann MB, Seufert PS, Schmidtborn LC. Perceptual relevance of abnormal visual field representations: static visual field perimetry in human albinism. *Br J Ophthalmol*. 2007; 91:509–513. [PubMed: 17372340]
- Hoffmann MB, Stadler J, Kanowski M, Speck O. Retinotopic mapping of the human visual cortex at a magnetic field strength of 7T. *Clin Neurophysiol*. 2009; 120:108–116. [PubMed: 19071059]
- Hoffmann MB, Tolhurst DJ, Moore AT, Morland AB. Organization of the visual cortex in human albinism. *J Neurosci*. 2003; 23:8921–8930. [PubMed: 14523094]
- Huang H, Zhang J, Jiang H, Wakana S, Poetscher L, Miller MI, van Zijl PC, Hillis AE, Wytik R, Mori S. DTI tractography based parcellation of white matter: application to the mid-sagittal morphology of corpus callosum. *NeuroImage*. 2005; 26:195–205. [PubMed: 15862219]
- Huberman AD, Feller MB, Chapman B. Mechanisms underlying development of visual maps and receptive fields. *Annual review of neuroscience*. 2008; 31:479–509.
- Jancke D, Chavane F, Naaman S, Grinvald A. Imaging cortical correlates of illusion in early visual cortex. *Nature*. 2004; 428:423–426. [PubMed: 15042090]
- Kanowski M, Rieger JW, Noesselt T, Tempelmann C, Hinrichs H. Endoscopic eye tracking system for fMRI. *Journal of neuroscience methods*. 2007; 160:10–15. [PubMed: 16978705]
- Klemen J, Hoffmann MB, Chambers CD. Cortical plasticity in the face of altered input to V1. *Cortex*. 2012 In press.
- Levin N, Dumoulin SO, Winawer J, Dougherty RF, Wandell BA. Cortical maps and white matter tracts following long period of visual deprivation and retinal image restoration. *Neuron*. 2010; 65:21–31. [PubMed: 20152110]
- Maes F, Collignon A, Vandermeulen D, Marchal G, Suetens P. Multimodality image registration by maximization of mutual information. *IEEE transactions on medical imaging*. 1997; 16:187–198. [PubMed: 9101328]
- Muckli L, Naumer MJ, Singer W. Bilateral visual field maps in a patient with only one hemisphere. *Proceedings of the National Academy of Sciences of the United States of America*. 2009; 106:13034–13039. [PubMed: 19620732]
- Nestares O, Heeger DJ. Robust multiresolution alignment of MRI brain volumes. *Magn Reson Med*. 2000; 43:705–715. [PubMed: 10800036]
- Pelli DG. The VideoToolbox software for visual psychophysics: transforming numbers into movies. *Spatial vision*. 1997; 10:437–442. [PubMed: 9176953]
- Petros TJ, Rebsam A, Mason CA. Retinal axon growth at the optic chiasm: to cross or not to cross. *Annual review of neuroscience*. 2008; 31:295–315.
- Prakash S, Dumoulin SO, Fischbein N, Wandell BA, Liao YJ. Congenital Achromatopsia and See-Saw Nystagmus in VACTERL Syndrome. *J Neuroophthalmol*. 2010; 30:45–48. [PubMed: 20182207]
- Rohde GK, Barnett AS, Basser PJ, Marengo S, Pierpaoli C. Comprehensive approach for correction of motion and distortion in diffusion-weighted MRI. *Magn Reson Med*. 2004; 51:103–114. [PubMed: 14705050]
- Rohde GK, Barnett AS, Basser PJ, Pierpaoli C. Estimating intensity variance due to noise in registered images: applications to diffusion tensor MRI. *NeuroImage*. 2005; 26:673–684. [PubMed: 15955477]
- Sereno MI, Dale AM, Reppas JB, Kwong KK, Belliveau JW, Brady TJ, Rosen BR, Tootell RB. Borders of multiple visual areas in humans revealed by functional magnetic resonance imaging. *Science*. 1995; 268:889–893. [PubMed: 7754376]

- Sherbondy AJ, Dougherty RF, Ben-Shachar M, Napel S, Wandell BA. ConTrack: finding the most likely pathways between brain regions using diffusion tractography. *Journal of vision* [electronic resource]. 2008a; 8:15, 11–16.
- Sherbondy AJ, Dougherty RF, Napel S, Wandell BA. Identifying the human optic radiation using diffusion imaging and fiber tractography. *Journal of vision* [electronic resource]. 2008b; 8:12 11–11.
- Silver MA, Ress D, Heeger DJ. Topographic maps of visual spatial attention in human parietal cortex. *Journal of neurophysiology*. 2005; 94:1358–1371. [PubMed: 15817643]
- Teo PC, Sapiro G, Wandell BA. Creating connected representations of cortical gray matter for functional MRI visualization. *IEEE transactions on medical imaging*. 1997; 16:852–863. [PubMed: 9533585]
- Van de Moortele PF, Auerbach EJ, Olman C, Yacoub E, Ugurbil K, Moeller S. T1 weighted brain images at 7 Tesla unbiased for Proton Density, T2\* contrast and RF coil receive B1 sensitivity with simultaneous vessel visualization. *NeuroImage*. 2009; 46:432–446. [PubMed: 19233292]
- Victor JD, Apkarian P, Hirsch J, Conte MM, Packard M, Relkin NR, Kim KH, Shapley RM. Visual function and brain organization in non-decussating retinal-fugal fibre syndrome. *Cereb Cortex*. 2000; 10:2–22. [PubMed: 10639391]
- Victor JD, Purpura K, Katz E, Mao B. Population encoding of spatial frequency, orientation, and color in macaque V1. *Journal of neurophysiology*. 1994; 72:2151–2166. [PubMed: 7884450]
- Wandell BA, Chial S, Backus BT. Visualization and measurement of the cortical surface. *Journal of cognitive neuroscience*. 2000; 12:739–752. [PubMed: 11054917]
- Wandell BA, Dumoulin SO, Brewer AA. Visual field maps in human cortex. *Neuron*. 2007; 56:366–383. [PubMed: 17964252]
- Williams RW, Hogan D, Garraghty PE. Target recognition and visual maps in the thalamus of chiasmatic dogs. *Nature*. 1994; 367:637–639. [PubMed: 8107846]
- Winawer J, Horiguchi H, Sayres RA, Amano K, Wandell BA. Mapping hV4 and ventral occipital cortex: the venous eclipse. *Journal of vision* [electronic resource]. 2010; 10:1–22.
- Wolynski B, Kanowski M, Meltendorf S, Behrens-Baumann W, Hoffmann MB. Self-organisation in the human visual system--visuo-motor processing with congenitally abnormal V1 input. *Neuropsychologia*. 2010; 48:3834–3845. [PubMed: 20863844]
- Zaitsev M, Hennig J, Speck O. Point spread function mapping with parallel imaging techniques and high acceleration factors: fast, robust, and flexible method for echo-planar imaging distortion correction. *Magn Reson Med*. 2004; 52:1156–1166. [PubMed: 15508146]



### Highlights

- In achiasma eyes project contralateral only yet support basic visual functions
- Human achiasma causes highly atypical alternative cortical organization
- Organization reflects unaltered large-scale connections beyond the geniculate
- Developmental mechanisms in human achiasma are conservative

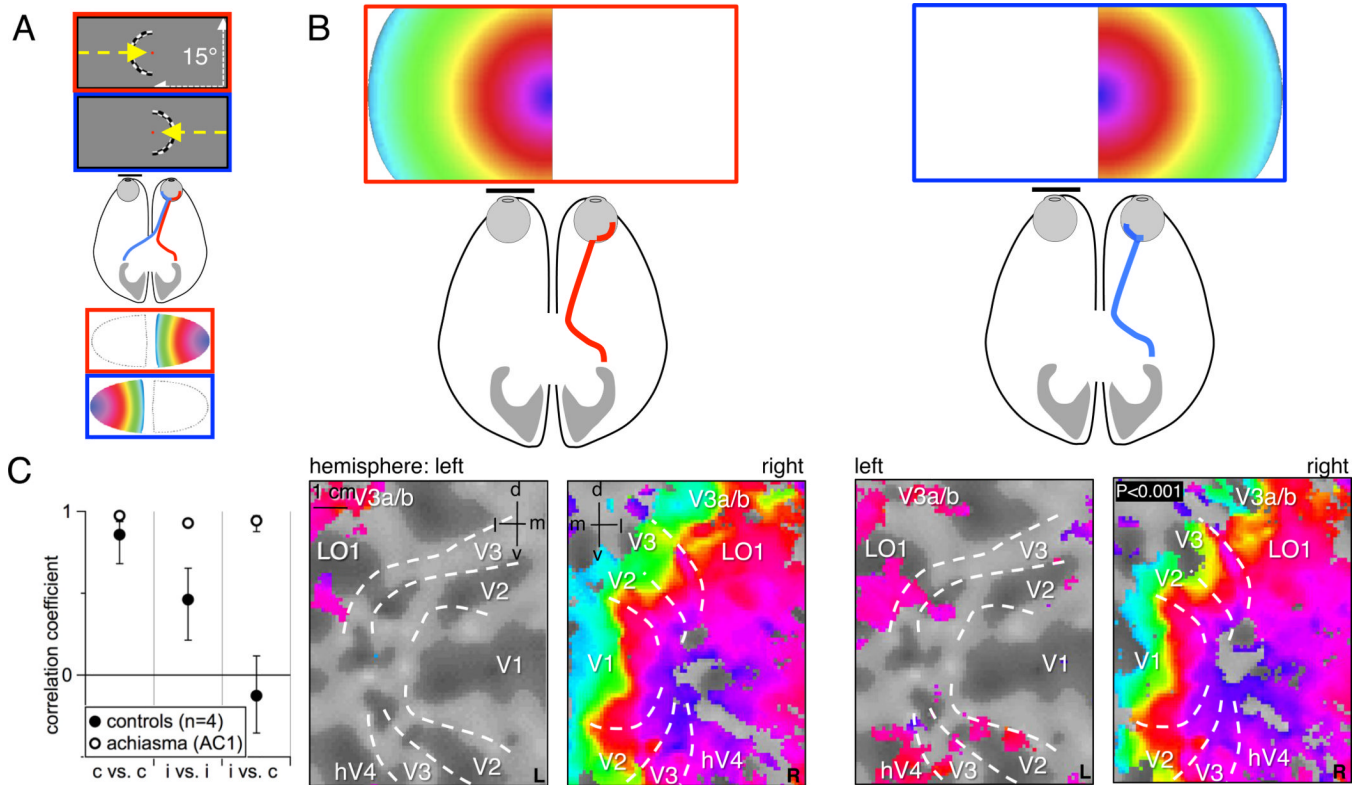


**Figure 1.**

Hemifield retinotopic mapping results. **A)** Schematic of the normal projection pattern of the optic nerve of the right eye together with the visual contracting ring stimulus for hemifield eccentricity and its color-coded lateralized representation in a schematic V1-flatmap. The nasal retina (blue) projects to the contralateral and the temporal retina (red) to the ipsilateral hemisphere, resulting in a representation of each hemifield on its respective contralateral hemisphere. **B)** Schematic of the achiasmic optic nerve projection and eccentricity maps in AC1's flattened representation of the early visual areas upon separate monocular stimulation of the right eye in the left and right visual hemifield. Responses are dominant in the right hemisphere and organized as an orderly eccentricity map for both visual hemifields. The visual area boundaries are indicated as determined from polar angle mapping (supplementary Figure S1). **C)** Correlation of the respective hemifield mappings to quantify the cortical superposition of hemifield maps in right V1 (mean±SD across four controls and for AC1 across repetitive correlations). In the controls the two repetitions of contralateral hemifield mappings were correlated ( $p<0.01$ ) and, to a lesser degree ( $p<0.04$ ), also those of two repetitions of ipsilateral hemifield mappings, but, in contrast, not those of contra- and ipsilateral field mappings. For AC1 both contra- and ipsilateral field mappings were highly correlated ( $p<0.001$ ). See also supplementary Figure S1.

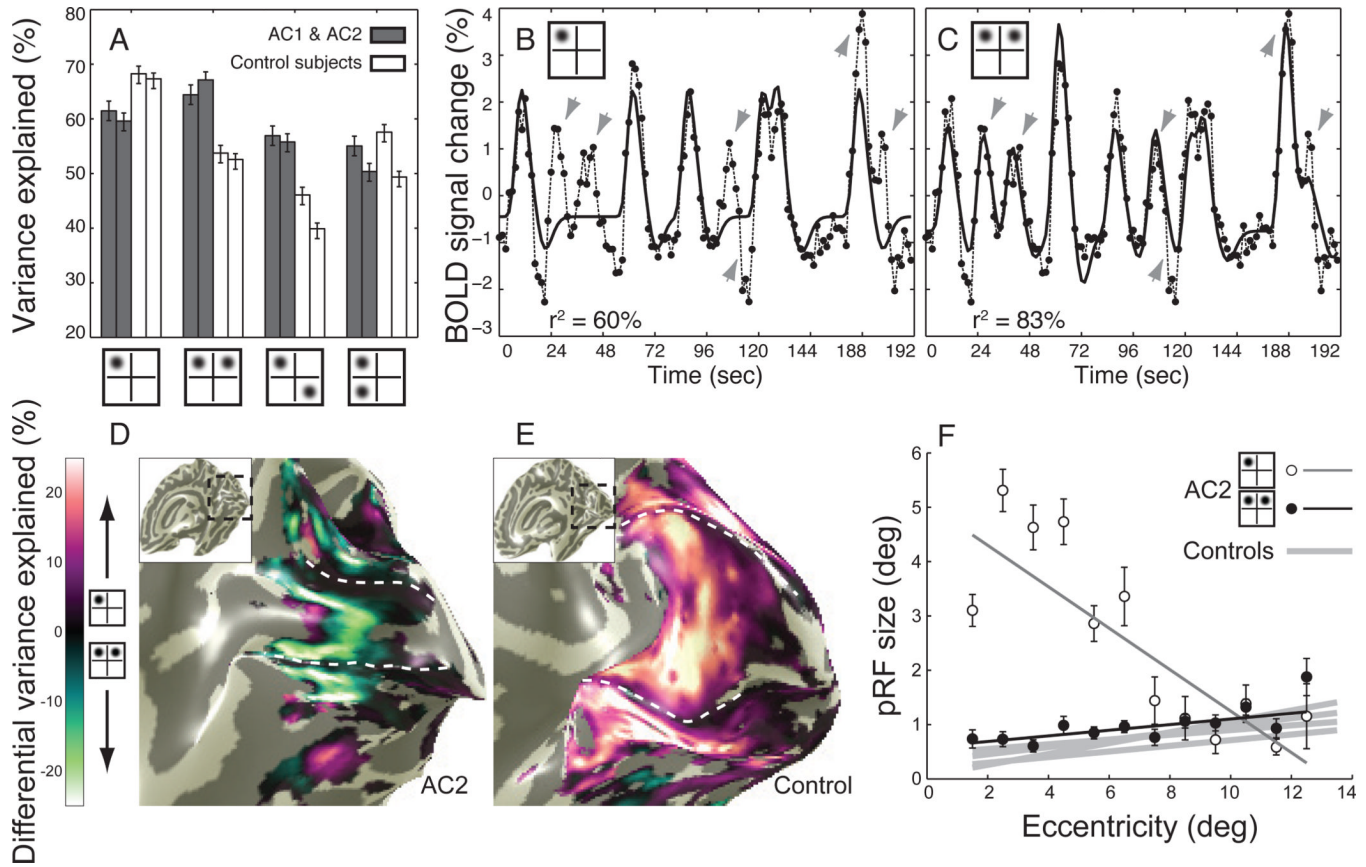


**Figure 2.** Population receptive field modelling results. **A)** pRF model comparisons for AC1 and AC2 (left and right, respectively) and two control subjects at the respective measurement sites. The mean variance explained and 95% confidence intervals for fMRI responses in the right Calcarine sulcus are shown for four different pRF models. Only cortical locations where any model explains more than 50% of the variance are included in the analysis. However the results are near-identical for any other or no threshold. Four different models were tested: the conventional pRF model containing 1 Gaussian, and three different pRF models with 2 Gaussians where the Gaussians are mirrored around the y-axis, fixation or x-axis. The pRF models are indicated by the x-axis' cartoon representations. There is no difference in degrees of freedom in the models. In the right hemisphere of the achiasmatic subjects, the model containing 2 pRFs mirrored around the y-axis explains most of the variance. In control subjects, the conventional model explains most of the variance in the data. Two example pRF model fits are shown in panels **B** and **C**. These panels show the fMRI data of AC2 (dotted line) fitted (solid line) with a conventional pRF using a single Gaussian (**B**) and a 2 Gaussian pRF model (**C**). The insets indicate the particular pRF model that is fitted to the data and the variance explained ( $r^2$ ). The conventional pRF model consistently misses certain time-series features that are captured by the 2 Gaussian pRF model (gray arrows). Next we compare the conventional pRF model to the pRF model consisting of 2 Gaussians mirrored on the y-axis by subtracting the variance explained of either model. The difference in percent variance explained of both models is shown on the cortical surfaces of AC2 (**D**) and a control subject (**E**). The data that is shown has at least a variance explained of 30% in any pRF model. The dashed white lines indicate the V1-V2 border (vertical meridian or Y-axis). In the subject without an optic chiasm the pRF model with two Gaussians mirrored on the Y-axis explains most of the variance within and beyond V1, whereas the in the control

subject the conventional model explains most of the variance in the fMRI data. **F)** pRF size versus eccentricity in the right Calcarine sulcus of AC2 and 4 control subjects. In the control subjects pRF sizes increase with eccentricity (Dumoulin and Wandell, 2008). This relationship is also plotted for the subject without an optic chiasm for two pRF models (conventional model: open circles; pRF model consisting of two Gaussians mirrored on the Y-axis: closed circles). The pRF sizes of the conventional pRF model deviate from the known relationship between (p)RF size and eccentricity in humans and animals, but the pRF sizes of the novel two Gaussian pRF model are consistent with the known relationship as illustrated by control subjects. See also supplementary Figure S2.

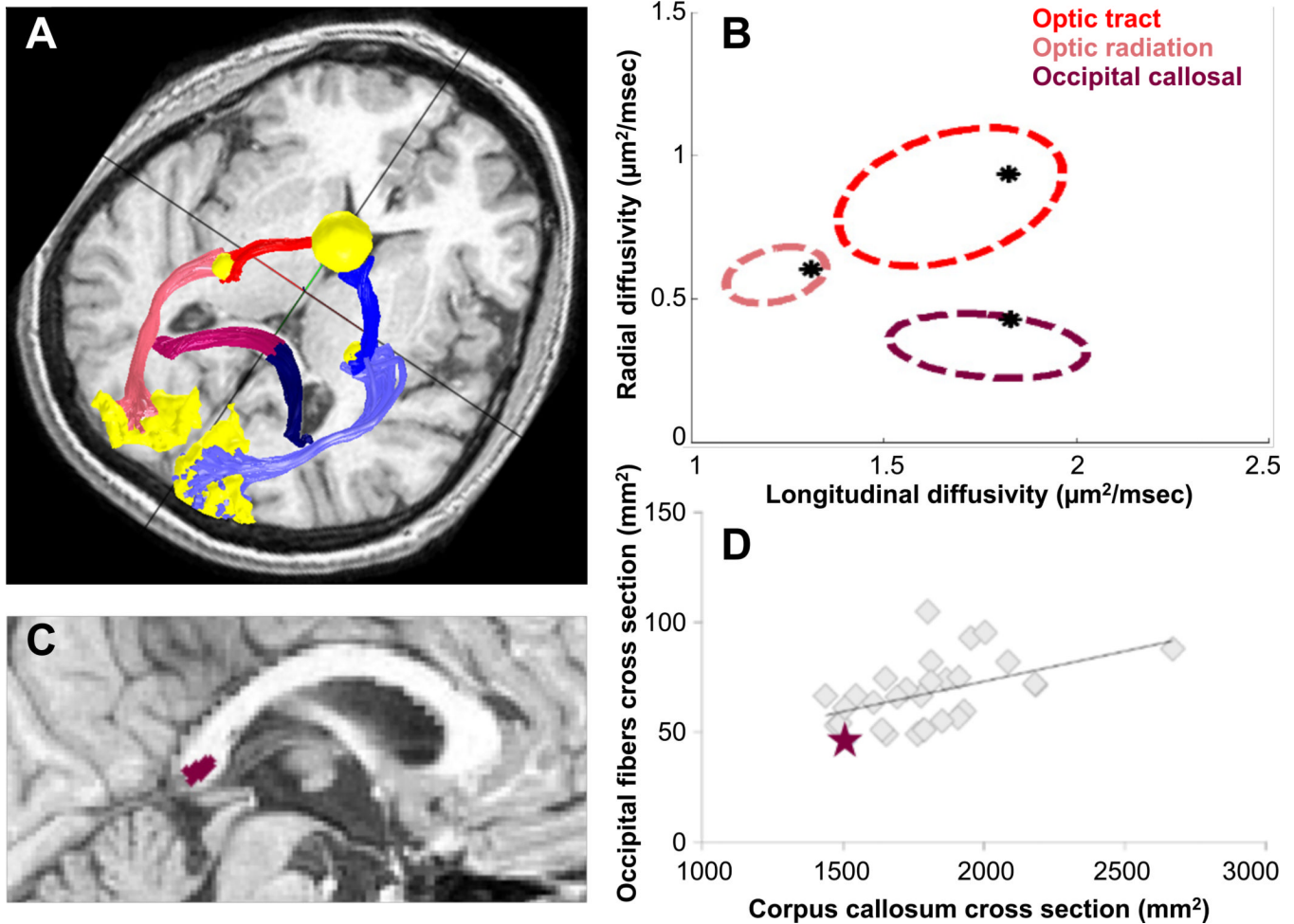


**Figure 3.**

Diffusion tensor imaging (DTI) and tractography results of AC2 and 30 controls. **(A)** ROIs and estimated fiber bundles superimposed on the T1 weighted axial slice, viewed from below. Estimates of the right (red) and left (blue) optic tracts; the right (pink) and left (purple) optic radiations; the right (dark red) and left (dark blue) occipital callosal fibers. Yellow spheres represent the optic chiasm (large anterior) LGN's (small in the middle) and Calcarine sulcus (posterior) regions of interest. **(B)** Scatter plot of the radial and longitudinal diffusivities of the optic tract, optic radiation and occipital callosal fiber groups (see color legend on the right). The 2 standard deviation covariance ellipsoid of 30 normally sighted subjects is drawn for each fiber group. The black stars represent the averaged right and left diffusivity values for each fiber group in the achiasmic subject which are within the range of control subjects. **(C)** The location of the occipital callosal fibers in the plane of the corpus callosum. **(D)** Scatter plot of the cross-sectional area of the occipital callosal fiber group in relation to the cross-sectional area of the entire corpus callosum. The cross-sectional area of achiasmic occipital callosal fiber group (purple star) is small compared to the controls (grey diamonds); however, the overall size of AC2's corpus callosum is small too.